IMPLEMENTING MULTI-SCALE AGRICULTURAL INDICATORS EXPLOITING SENTINELS

VEGETATION FIELD DATA AND PRODUCTION OF GROUND-BASED MAPS:

PSHENICHNE SITE, UKRAINE
14TH MAY, 15TH JUNE AND 15TH JULY 2013

ISSUE I1.10

EC Proposal Reference N° FP7-311766

Actual submission date : November 2013

Start date of project: 01.11.2012 Duration : 40 months

Name of lead partner for this deliverable: EOLAB

Book Captain: Consuelo Latorre (EOLAB)

Contributing Authors: Jorge Sánchez, Fernando Camacho (EOLAB)
Natalia Kussul, Skakun Serhiy, Kravchenko Oleksiy
(Space Research Institute NAS Ukraine and SSA Ukraine)

Project co-funded by the European Commission within the Seventh Framework Program (2007-2013)		
Dissemination Level		
PU	Public	**X**
PP	Restricted to other programme participants (including the Commission Services)	
RE	Restricted to a group specified by the consortium (including the Commission Services)	
CO	Confidential, only for members of the consortium (including the Commission Services)	

DOCUMENT RELEASE SHEET

Book Captain:	C. Latorre	Date: 29.11.2013	Sign. 
Approval:	R. Lacaze	Date: 03.04.2014	Sign 
Endorsement:	V. Puzzolo	Date:	Sign.
Distribution:			

CHANGE RECORD

Issue/Revision	Date	Page(s)	Description of Change	Release
	04.10.2013	All	First Issue	I1.00
	29.11.2013	All	A third campaign (July, 2013) has been included	I1.10

TABLE OF CONTENTS

LIST OF FIGURES

LIST OF TABLES

1. BACKGROUND OF THE DOCUMENT

1.1. EXECUTIVE SUMMARY

The Copernicus Land Service has been built in the framework of the FP7 geoland2 project, which has set up pre-operational infrastructures. ImagineS intends to ensure the continuity of the innovation and development activities of geoland2 to support the operations of the global land component of the GMES Initial Operation (GIO) phase. In particular, the use of the future Sentinel data in an operational context will be prepared. Moreover, IMAGINES will favor the emergence of new downstream activities dedicated to the monitoring of crop and fodder production.

The main objectives of ImagineS are to (i) improve the retrieval of basic biophysical variables, mainly LAI, FAPAR and the surface albedo, identified as Terrestrial Essential Climate Variables, by merging the information coming from different Sentinel sensors and other Copernicus contributing missions; (ii) develop qualified software able to process multi-sensor data at the global scale on a fully automatic basis; (iii) propose an original agriculture service relying upon a new method to assess the biomass, based on the assimilation of satellite products in a Land Data Assimilation System (LDAS) in order to monitor the crop/fodder biomass production together with the carbon and water fluxes; (iv) demonstrate the added value of this agriculture service for a community of users acting at global, European, national, and regional scales.

Further, ImagineS will serve the growing needs of international (e.g. FAO and NGOs), European (e.g. DG AGRI, EUROSTATS, DG RELEX), and national users (e.g. national services in agro-meteorology, ministries, group of producers, traders) on accurate and reliable information for the implementation of the EU Common Agricultural Policy, of the food security policy, for early warning systems, and trading issues. ImagineS will also contribute to the Global Agricultural Geo-Monitoring Initiative (GEO-GLAM) by its original agriculture service which can monitor crop and fodder production together with the carbon and water fluxes and can provide drought indicators, and through links with JECAM (Joint Experiment for Crop Assessment and Monitoring).

1.2. PORTFOLIO

The ImagineS portfolio contains global and regional biophysical variables derived from multi-sensor satellite data, at different spatial resolutions, together with agricultural indicators, including the above-ground biomass, the carbon and water fluxes, and drought indices resulting from the assimilation of the biophysical variables in the Land Data Assimilation System (LDAS). The ambition of the project is to provide a full coverage of the globe, at a frequency of 10 days, merging Sentinel-3 and Proba-V data.

1.3. SCOPE AND OBJECTIVES

The main objective of this document is to describe the ground database provided by the Space Research Institute NAS and SSA Ukraine, and the processing carried out by EOLAB to derive high resolution maps of the following biophysical variables:

- Leaf Area Index: Two LAI maps are produced per campaign, the first one corresponds to effective LAI (LAIeff) derived from the description of the gap fraction as a function of the view zenith angle, and the second one (LAItrue) which is derived from the LAIeff and the clumping factor.
- Fraction of Vegetation Cover (FCOVER): defined as the proportion of soil covered by vegetation, derived from the gap fraction between 0 and 10º of view zenith angle.
- Fraction of Absorbed Photosynthetically Active Radiation (FAPAR): It is the fraction of the photosynthetically active radiation (PAR) absorbed by a vegetation canopy. PAR is the solar radiation reaching the canopy in the 0.4–0.7 µm wavelength region. The derivation of FAPAR from CAN-EYE corresponds to the instantaneous black sky FAPAR at 10h00 AM.

1.4. CONTENT OF THE DOCUMENT

This document is structured as follows:

- Chapter 2 provides an introduction to the field experiment.
- Chapter 3 provides the location and description of the site.
- Chapter 4 describes the ground measurements, including material and methods, sampling and data processing.
- Chapter 5 describes an evaluation of the sampling.
- Chapter 6 describes the methodology to derive high resolution maps of the biophysical variables, and the results of the high resolution dataset.
- Finally, conclusions and references are given.

2. INTRODUCTION

Validation of remote sensing products is mandatory to guaranty that the satellite products meets the user's requirements. Protocols for validation of global LAI products are already developed in the context of Land Product Validation (LPV) group of the Committee on Earth Observation Satellite (CEOS) for the validation of satellite-derived land products (Fernandes et al., 2012), and recently applied to Copernicus global land products based on SPOT/VGT observation (Camacho et al., 2013). This generic approach is made of 2 major components:

- The indirect validation: including inter-comparison between products as well as evaluation of their temporal and spatial consistency
- The direct validation: comparing satellite products to ground measurements of the corresponding biophysical variables. In the case of low and medium resolution sensors, the main difficulty relies on scaling local ground measurements to the extent corresponding to pixels size. However, the direct validation is limited by the small number of sites, for that reason a main objective of ImagineS is the collection of ground truth data in demonstration sites.

The content of this document is compliant with existing validation guidelines (the generation for up-scaling ground maps for direct validation) as proposed by the CEOS LPV group (Morisette et al., 2006); the VALERI project (http://w3.avignon.inra.fr/valeri/) and ESA campaigns (Baret and Fernandes, 2012). It therefore follows the general strategy based on a bottom up approach: it starts from the scale of the individual measurements that are aggregated over an elementary sampling unit (ESU) corresponding to a support area consistent with that of the high resolution imagery used for the upscaling of ground data. Several ESUs are sampled over the site. Radiometric values over a decametric image are also extracted over the ESUs. This will be later used to develop empirical transfer functions for upscaling the ESU ground measurements (e.g. Martínez et al., 2009). Finally, the high resolution ground based map will be compared with the medium resolution satellite product at the spatial support of the product.

Three field campaigns to characterize the vegetation biophysical parameters at the Pshenichne test site were carried out by the Space Research Institute NAS and SSA Ukraine in the framework of JECAM (Joint Experiment for Crop Assessment and Monitoring) initiative

First campaign: 14th to 17th of May 2013.

Second campaign: 12th to 15th of June 2013.

Third campaign: 14th to 17th of July 2013.

Team involved in field collection:

Natalia Kussul, Skakun Serhiy, Kravchenko Oleksiy

Contact: Natalia Kussul (kussul@mail.ru)

3. STUDY AREA

3.1. LOCATION

The experimental site is located around Pshenichne farm. Pshenichne is located in the region of Kiev, 50 km away from the capital. Crop types in this region are typically winter wheat, spring barley, maize, soy beans, winter rapeseed, sunflower, sugar beet, potatoes, winter rye, and spring wheat. Due to the relatively large number of major crops and other factors, there is no a typical simple crop rotation in this region. Most producers use different crop rotations depending on specialization. The crop calendar is September-July for winter crops and April-October for spring and summer crops. The climatic zone is humid continental.

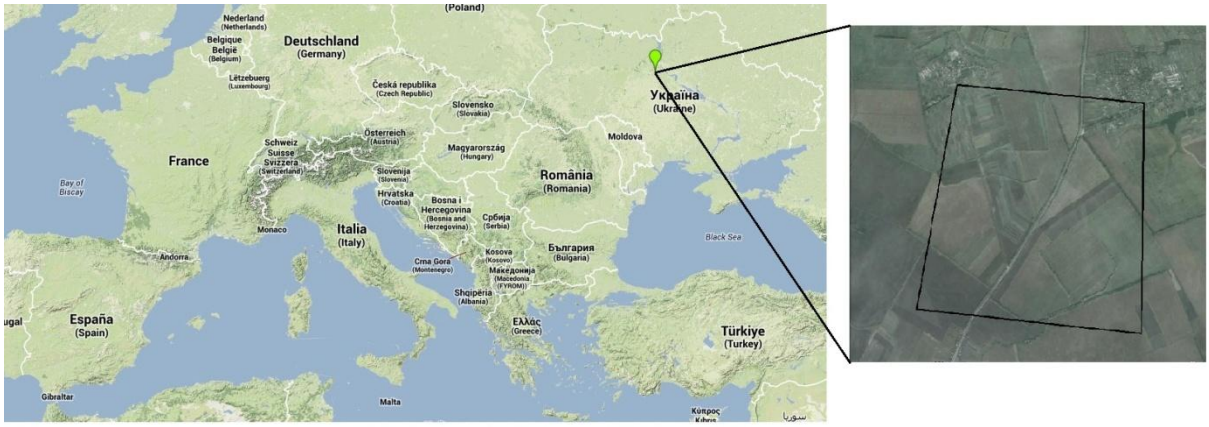

Figure 1: Location of Pshenichne site in Ukraine (left side). The selected 3x3 km^2 study area (right side)

The study area (Figure 1) is defined by a 3x3 km^2 region around the central coordinate (Table 1).

Table 1: Coordinates and altitude of the test site.

Site Center	
Geographic Lat/lon, WGS-84 (degrees)	Latitude = 50.07656834° N Longitude = 30.23223886° E
Altitude	200 m

3.2. DESCRIPTION OF THE TEST SITE.

Figure 2 shows the land use map during the field campaigns. Land cover changes are observed in some field plots. The 3x3km^2 area in the Pshenichne site is mainly occupied by sun flower, maize and grassland.

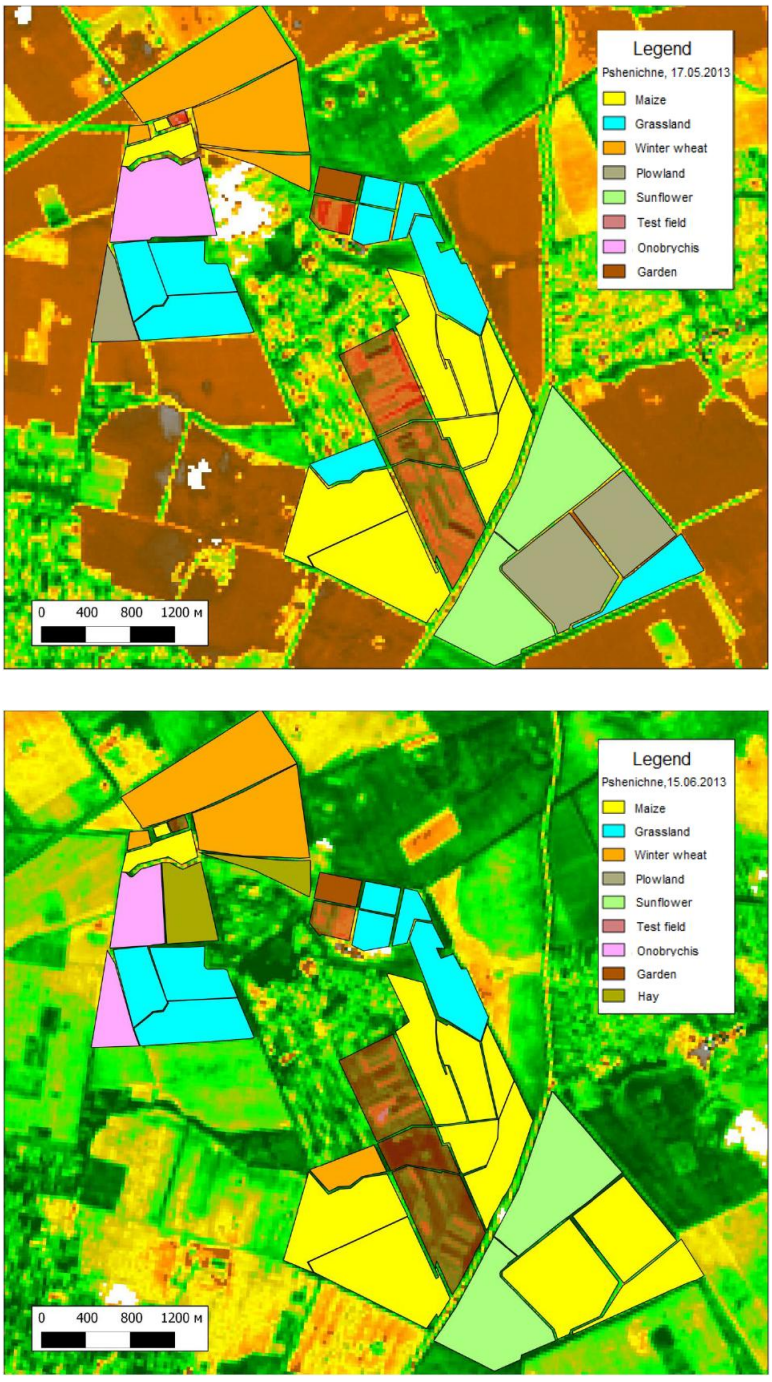

Figure 2: Land use map of the study area. Top: First campaign (May). Bottom: Second campaign (June). Land cover map for the third campaign was not provided.

4. GROUND MEASUREMENTS

The ground measurement database was acquired and provided by the Space Research Institute NAS Ukraine and SSA Ukraine.

4.1. MATERIAL AND METHODS

Digital Hemispheric Photographs (DHP) were acquired with a NIKON D70 camera. Hemispherical photos allow the calculation of LAI and FCOVER measuring gap fraction through an extreme wide-angle camera lens (i.e. 180º) (Weiss et al., 2004). It produces circular images that record the size, shape, and location of gaps, either looking upward from within a canopy or looking downward from above the canopy.

The hemispherical images acquired during the field campaign are processed with the CAN-EYE software (http://www.avignon.inra.fr/can_eye) to derive LAI, FAPAR and FCOVER. It is based on a RGB colour classification of the image to discriminate vegetation elements from background (i.e., gaps). This approach allows exploiting downward-looking photographs for short canopies (background = soil) as well as upward-looking photographs for tall canopies (background = sky). Can-Eye software processes simultaneously up to of N = 16 images acquired over the same ESU. Note that the N images were acquired with similar illumination conditions to limit the variation of colour dynamics between images.

The CAN-EYE software computes biophysical variables from gap fraction as follows:

Effective LAI (LAIeff) is computed from the gap fraction Po,CAN_EYE(θ) following the Poisson law (Welles and Norman, 1991):

$$P_{0,CAN_{EYE(\theta)}} = \frac{e^{-L_{eff} \cdot G\left(\theta,\varphi,\theta_{leaf,eff}\right)}}{COS\theta} \qquad \text{Eq. (1)}$$

where θ and φ are respectively the zenith and azimuth angles of the direction of propagation of the incident beam, Leff refers to effective LAI, G is the mean projection of a leaf area unit in a plane perpendicular to direction (θ,φ) which is directly dependent of the leaf angle distribution (LAD). LAD is assumed to be uniform in azimuth and following an ellipsoidal distribution for the inclination. It is thus fully characterized with the average leaf angle (ALA) only. Two variables are therefore needed to describe canopy architecture under these assumptions: the effective LAI (Leff) and effective ALA ($\theta_{leaf,eff}$). A look-up-table (LUT) is used to estimate Leff and $\theta_{leaf,eff}$ from the measured zenithal variation of the gap fraction (Weiss et al., 2004).

Actual **LAI** that can be measured only using a planimeter with however possible allometric relationships to reduce the sampling are related to the effective leaf area index through:

$$LAI_{eff} = \lambda_0 \cdot LAI \qquad \text{Eq. (2)}$$

Where λ_0 is the clumping index. In CAN-EYE, the clumping index is computed using the Lang and Xiang (1986) logarithm gap fraction averaging method, although some uncertainties are associated to this method (Demarez et al., 2008). The principle is based on the assumption that vegetation elements are locally assumed randomly distributed. Values of clumping index given by CAN_EYE are in certain cases correlated with the size of the cells used to divide photographs. The values reported here were estimated with the CAN-EYE 5.1.

FCOVER, is retrieved from gap fraction between 0 to 10°.

$$FCOVER = 1 - P_0 \cdot (0 - 10°) \qquad \text{Eq. (3)}$$

FAPAR. As there is little scattering by leaves in that particular spectral domain due to the strong absorbing features of the photosynthetic pigments, FAPAR is often assumed to be equal to FIPAR (Fraction of Intercepted Photosynthetically Active Radiation), and therefore to the gap fraction. The actual FAPAR is the sum of two terms, weighted by the diffuse fraction in the PAR domain: the 'black sky' FAPAR that corresponds to the direct component and the 'white sky' or the diffuse component. Black-sky FAPAR is computed at 10:30 am, which is a good approximation of the daily integrated FAPAR value.

4.2. SPATIAL SAMPLING SCHEME

A total of 31, 34 and 37 ESUs were characterized during the first, second and third campaign. A pseudo-regular sampling was used within each ESU of approximately 20x20 m^2. The centre of the ESU was geo-located using a GPS. The number of hemispherical photos per ESU ranges between 12 and 15.

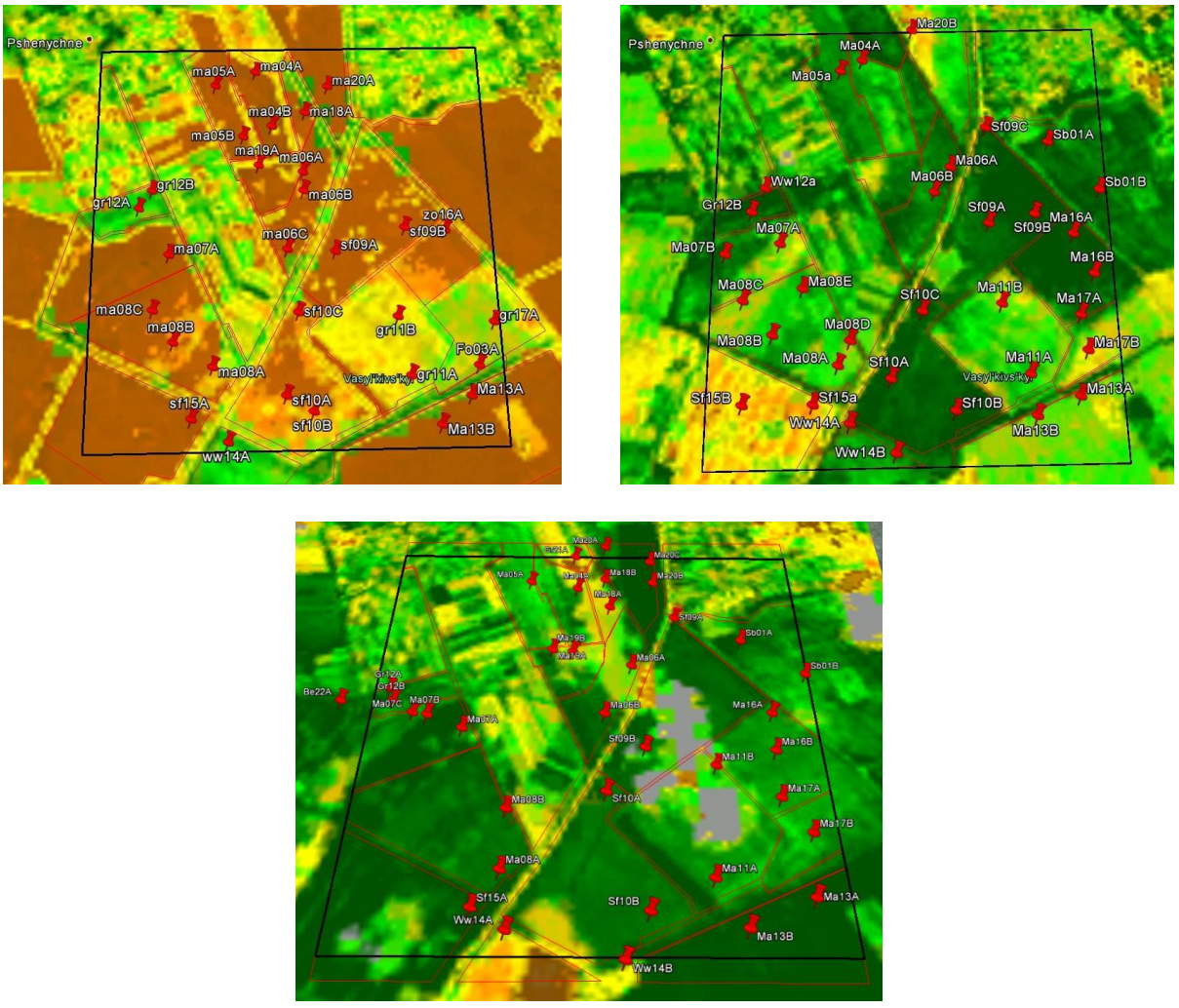

Figure 3: Distribution of the sampling units in the study area (3x3km^2). Top Left: First campaign (May). Top Right: Second campaign (June). Bottom: Third campaign (July).

4.1. CONTENT OF THE GROUND DATASET

Each ESU is described according to an agreed format. For this purpose a template file has been used (Table 2).

Table 2: The File template used to describe ESUs with the ground measurements.

Column	Var.Name		Comment
1	Plot #		Number of the field plot in the site
2	Plot Label		Label of the plot in the site
3	ESU #		Number of the Elementary Sampling Unit (ESU)
4	ESU Label		Label of the ESU in the campaign
5	Northing Coord.		Geographical coordinate: Latitude (º), WGS-84
6	Easting Coord.		Geographical coordinate: Longitude (º), WGS-84
7	Extent (m) of ESU (diameter)		Size of the ESU [(1)]
8	Land Cover		Detailed land cover
9	Start Date (dd/mm/yyyy)		Starting date of measurements
10	End Date (dd/mm/yyyy)		Ending date of measurements
11+4*j (*)	LAI	Method	Instrument
12+4j (*)		Nb. Replications	Number of Replications
13+4*j (*)		PRODUCT	Methodology
14+4*j (*)		Uncertainty	Standard deviation

(*)j=0:4. For LAI, LAIeff, FAPAR, FCOVER

Table 3 summarizes the number of sampling units (ESUs) per each crop type acquired during the three field campaigns.

Table 3: Summary of the field measurements in Pshenichne site.

Land Use	Number of ESU's		
	First Campaign (14^{th} - 17^{th} of May, 2013)	Second Campaign (12^{th} - 15^{th} of June, 2013)	Third Campaign (14^{th} - 17^{th} of July, 2013)
Sunflower (Sf)	6	8	5
Maize (Ma)	16	20	24
Grassland (Gr)	5	1	3
Winter Wheat (Ww)	1	3	2
Forest (Fo)	2	-	-
Plowed land (Zo)	1	-	
Beet (Be)	-	-	1
Soy Beans (Sb)	-	2	2
TOTAL	**31**	**34**	**37**

Figures 4, 5 and 6 show the measurements obtained during the field experiment. Figure 7 and 8 show the distribution of measurements. Distribution of LAI values are around 1 for the second campaign and below 0.5 for the first campaign. The available FCOVER and FAPAR measurements cover the full range of variation [0-1].

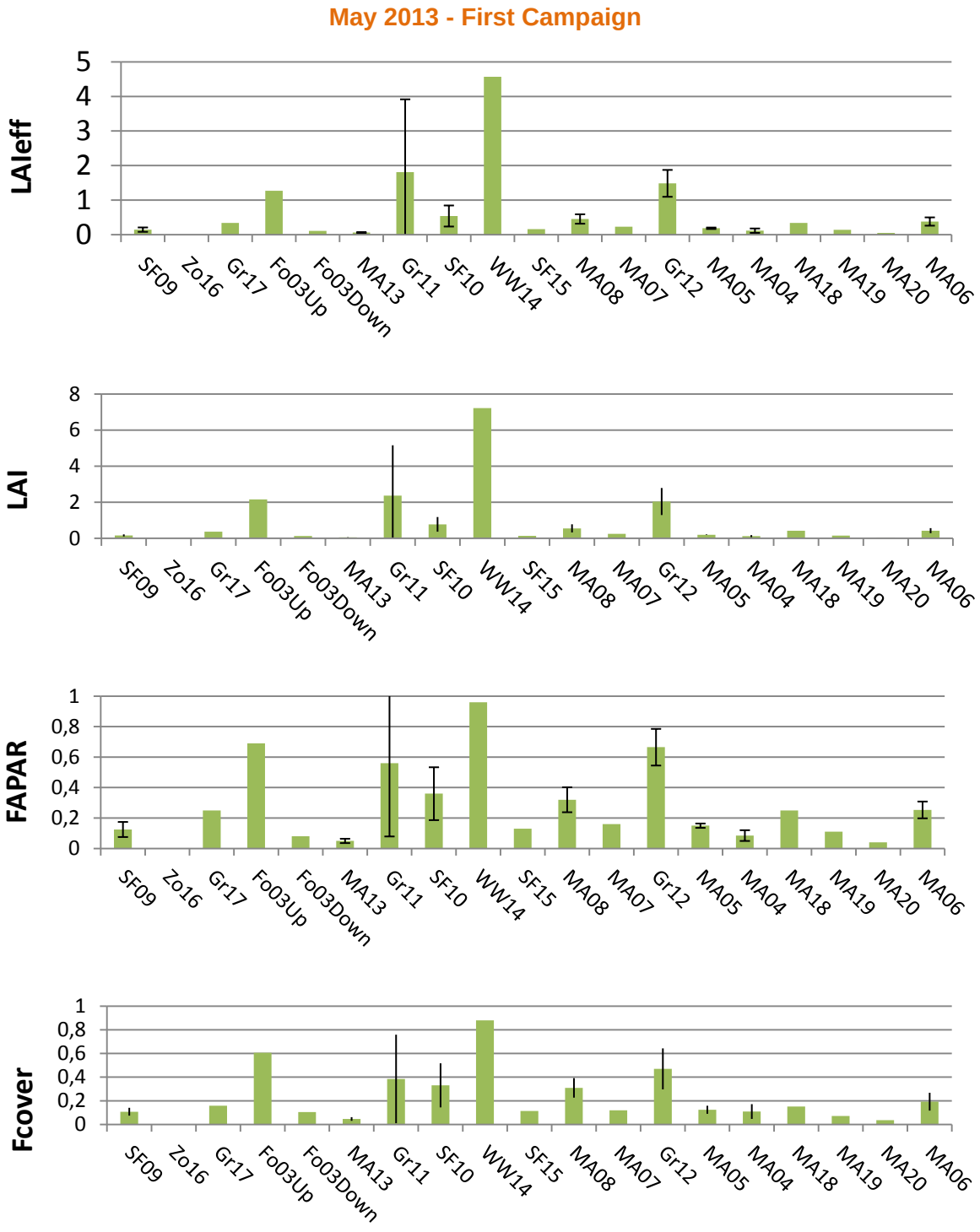

Figure 4: LAIeff, LAI, FAPAR and FCOVER measurements acquired in Pshenichne site during the first campaign (May, 2013). Mean values and standard deviation over each crop field are shown.

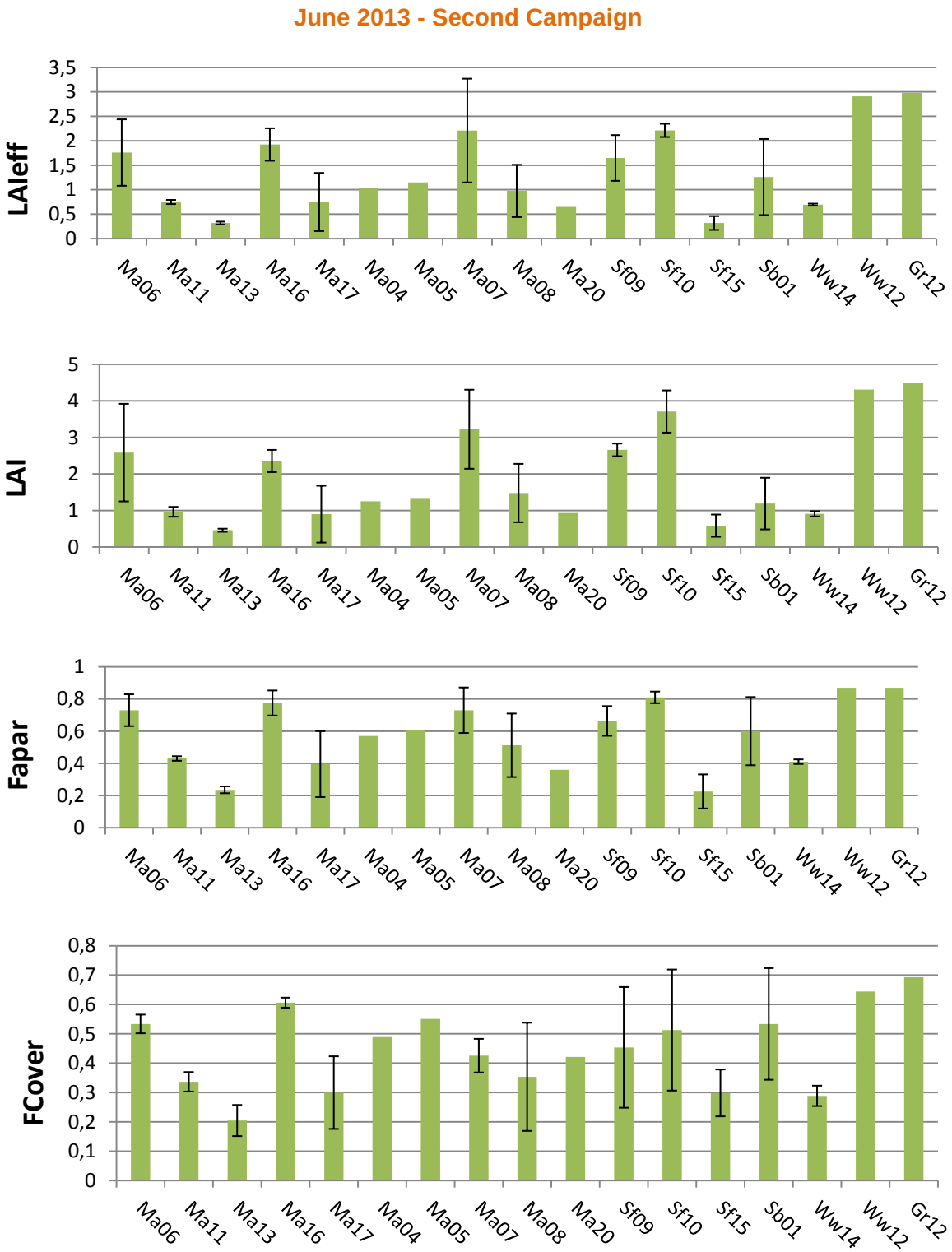

Figure 5: LAIeff, LAI, FAPAR and FCOVER measurements acquired in Pshenichne site during the second campaign (June). Mean values and its standard deviation over each crop field are shown.

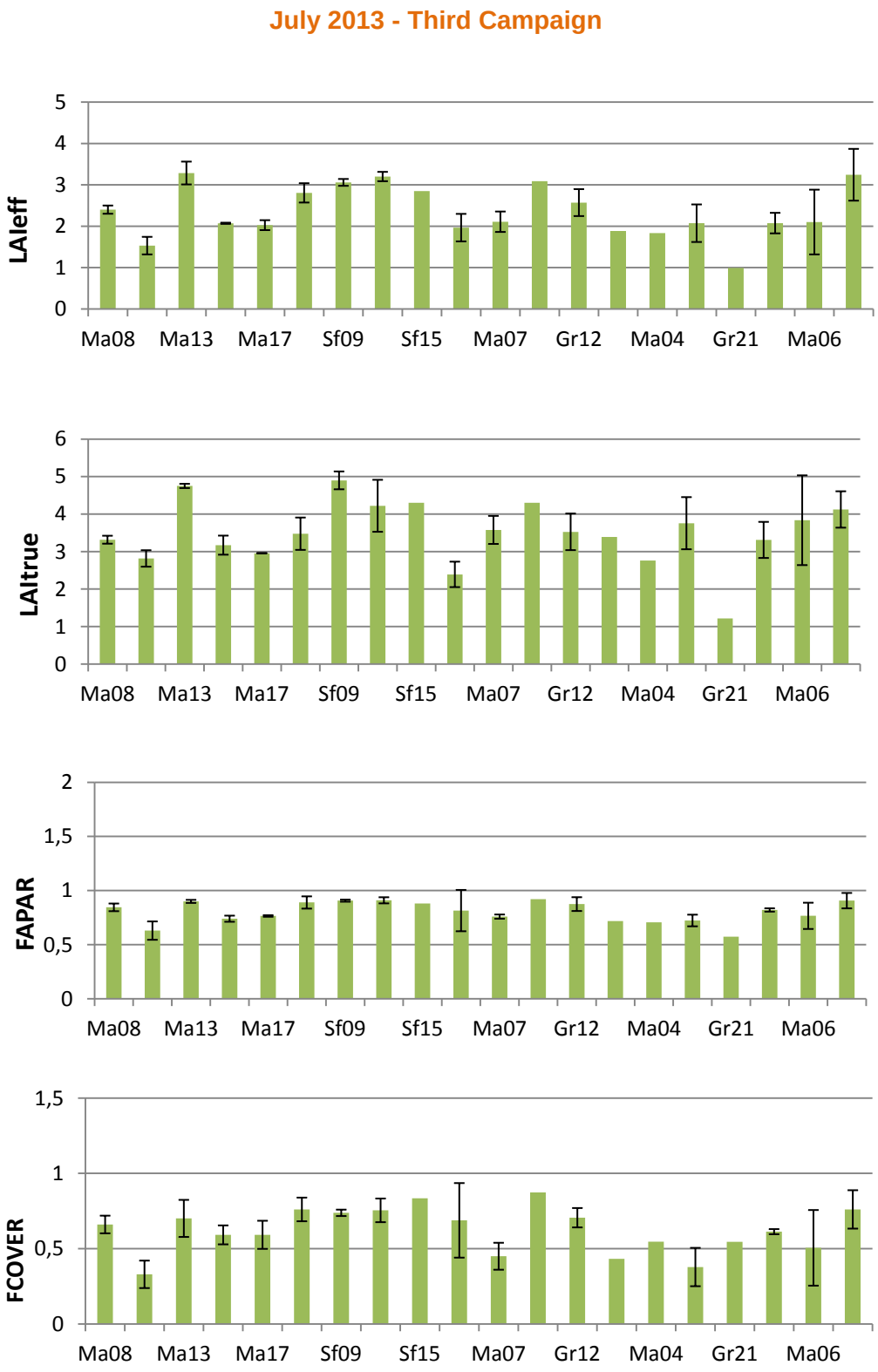

Figure 6: LAIeff, LAI, FAPAR and FCOVER measurements acquired in Pshenichne site during the third Campaign (July). Mean values and standard deviation over each crop field are shown.

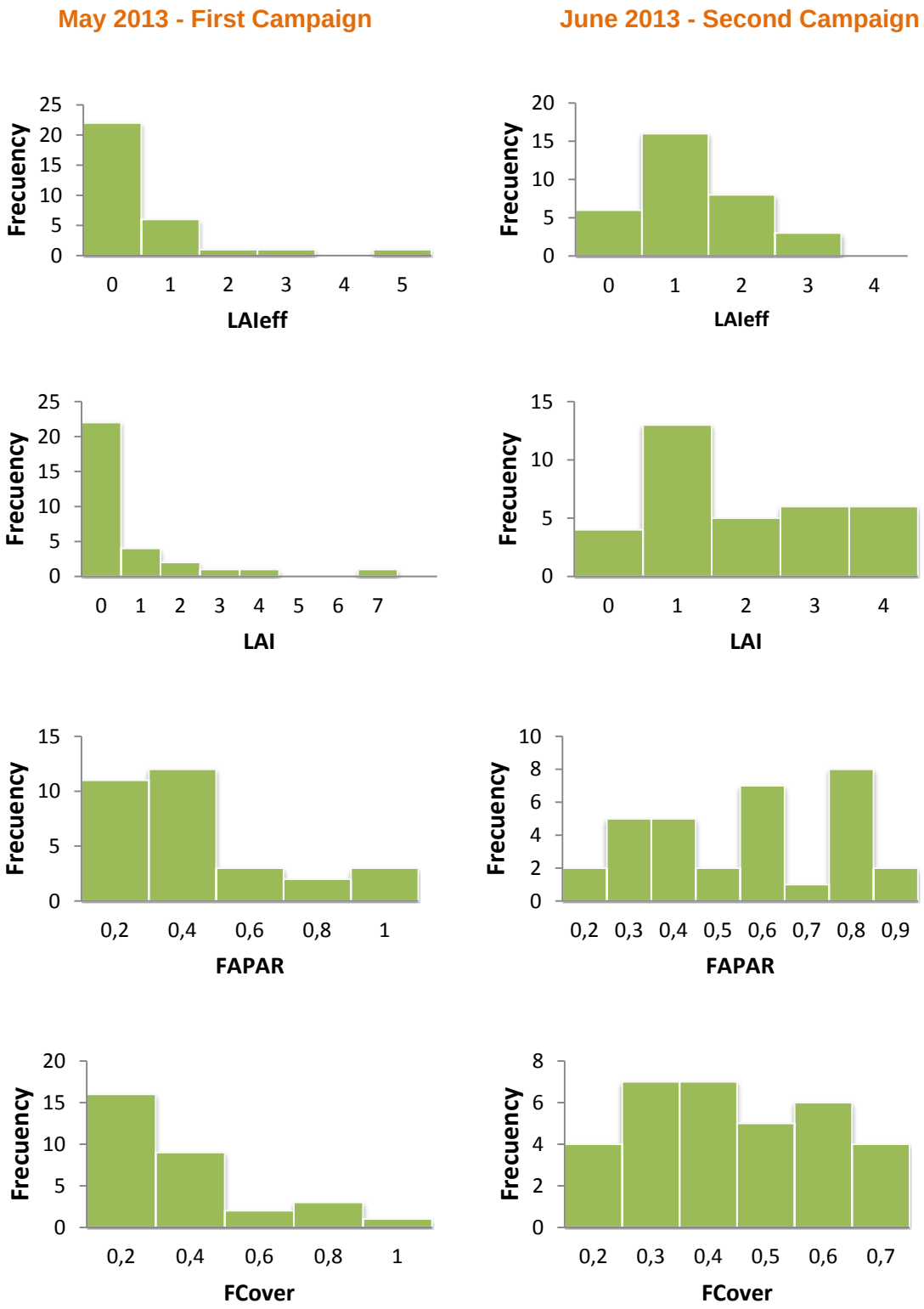

Figure 7: Distribution of the measured biophysical variables over the ESUs. Left: First campaign (May). Right: Second campaign (June).

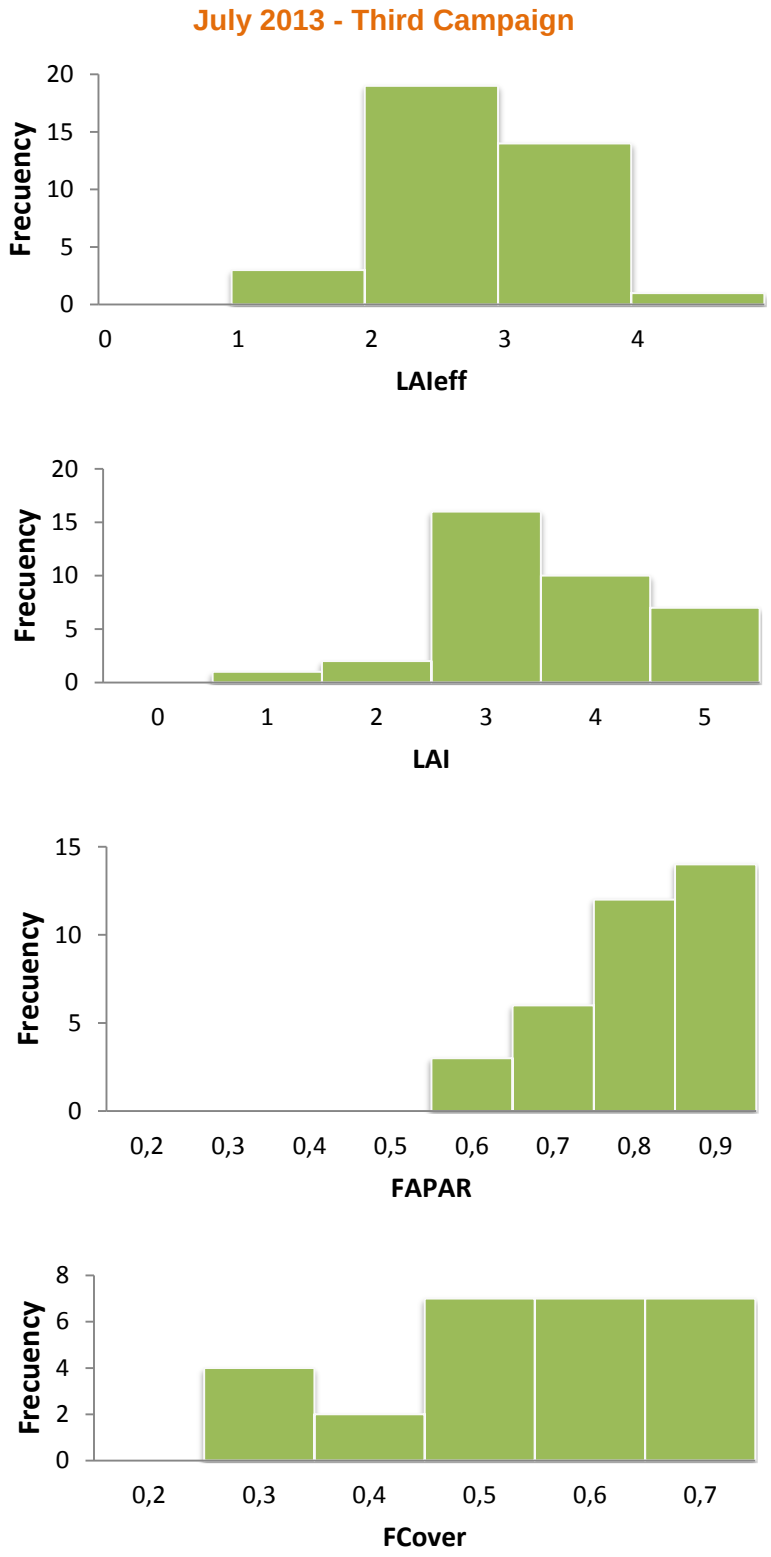

Figure 8: Distribution of the measured biophysical variables over the ESUs. Third campaign (July).

5. EVALUATION OF THE SAMPLING

5.1. PRINCIPLES

Based on previous field activities, the data set sampling was concentrated in the most representative crops. The number of ESUs was of 31, 34 and 37 for the first, second and third second campaigns respectively.

5.2. EVALUATION BASED ON NDVI VALUES

The sampling strategy is evaluated using the SPOT5 image by comparing the NDVI distribution over the site with the NDVI distribution over the ESUs (Figure 9 and Figure 10). As the number of pixels is drastically different for the ESU and whole site (WS) it is not statistically consistent to directly compare the two NDVI histograms. Therefore, the proposed technique consists in comparing the NDVI cumulative frequency of the two distributions by a Monte-Carlo procedure which aims at comparing the actual frequency to randomly shifted sampling patterns. It consists in:

1. computing the cumulative frequency of the *N* pixel NDVI that correspond to the exact ESU locations; then, applying a unique random translation to the sampling design (modulo the size of the image)

2. computing the cumulative frequency of NDVI on the randomly shifted sampling design

3. repeating steps 2 and 3, 199 times with 199 different random translation vectors.

This provides a total population of $N = 199 + 1$(actual) cumulative frequency on which a statistical test at acceptance probability $1 - \alpha = 95\%$ is applied: for a given NDVI level, if the actual ESU density function is between two limits defined by the $N\alpha / 2 = 5$ highest and lowest values of the 200 cumulative frequencies, the hypothesis assuming that WS and ESU NDVI distributions are equivalent is accepted, otherwise it is rejected.

Figure 9 shows that the NDVI distribution of the first and second campaign is good over the whole site (comprised between the 5 highest and lowest cumulative frequencies). Figure 10 shows that the NDVI distribution of the sampling of the third campaign (July) is closer to the lowest cumulative frequencies. This trend means that the sampling could present a slight bias towards high values of vegetation.

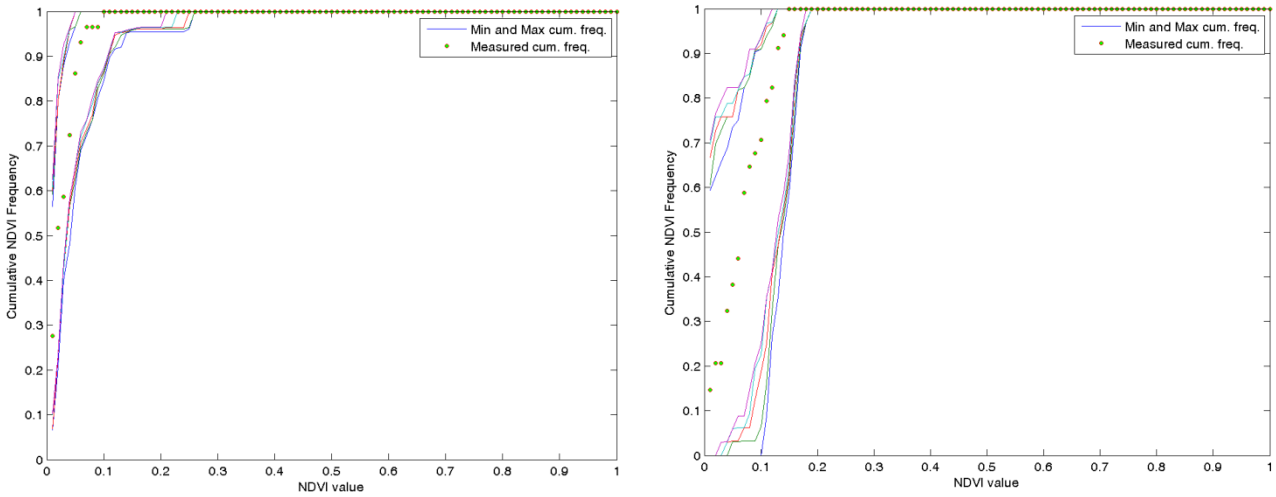

Figure 9: Comparison of NDVI distribution between ESUs (green dots) and over the whole image (blue line). Left: First Campaign (May). Right: Second Campaign (June).

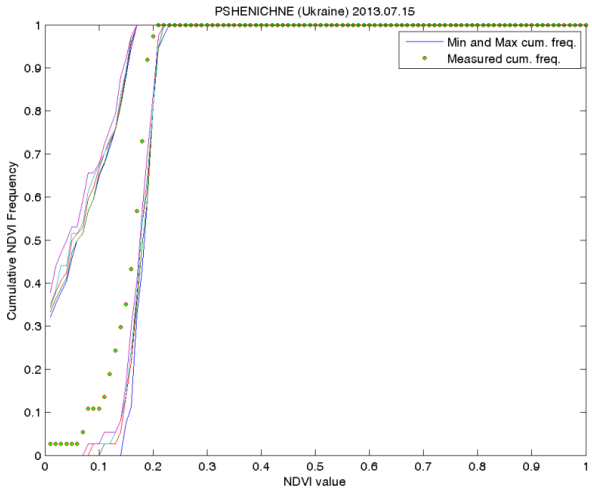

Figure 10: Comparison of NDVI distribution between ESUs (green dots) and over the whole image (blue line). Third Campaign (July).

5.3. EVALUATION BASED ON CONVEX HULL: PRODUCT QUALITY FLAG.

The interpolation capabilities of the empirical transfer function used for up-scaling the ground data using decametric images is dependent of the sampling (Martinez et al., 2009). A test based on the convex hulls was also carried out to characterize the representativeness of ESUs and the reliability of the empirical transfer function using the four selected bands (green, red, NIR and SWIR) of the SPOT5 image. A flag images is computed over the reflectances. The result on convex-hulls can be interpreted as:

● pixels inside the ‘strict convex-hull’: a convex-hull is computed using all the SPOT5 reflectances corresponding to the ESUs belonging to the class. These pixels are well represented by the ground sampling and therefore, when applying a transfer function the degree of confidence in the results will be quite high, since the transfer function will be used as an interpolator;

● pixels inside the ‘large convex-hull’: a convex-hull is computed using all the reflectance combinations (±5% in relative value) corresponding to the ESUs. For these pixels, the degree of confidence in the obtained results will be quite good, since the transfer function is used as an extrapolator (but not far from interpolator);

● pixels outside the two convex-hulls: this means that for these pixels, the transfer function will behave as an extrapolator which makes the results less reliable. However, having a priori information on the site may help to evaluate the extrapolation capacities of the transfer function.

The Figure 11 and 12 show the results of the Convex-Hull test (i.e., Quality Flag image) for the Pshenichne site over a 20x20 km^2 area around the central coordinate site. The convex hull map shows that the representativeness of the ESUs is relatively good as the pixels inside the strict and large convex-hulls are numerous in a 3x3 km^2 area (73% , 83% and 87 % for the first, second and third campaigns). This representativeness has been extended over a 20x20km^2 area, showing greater confidence in the third campaign (higher interpolation: blue color).

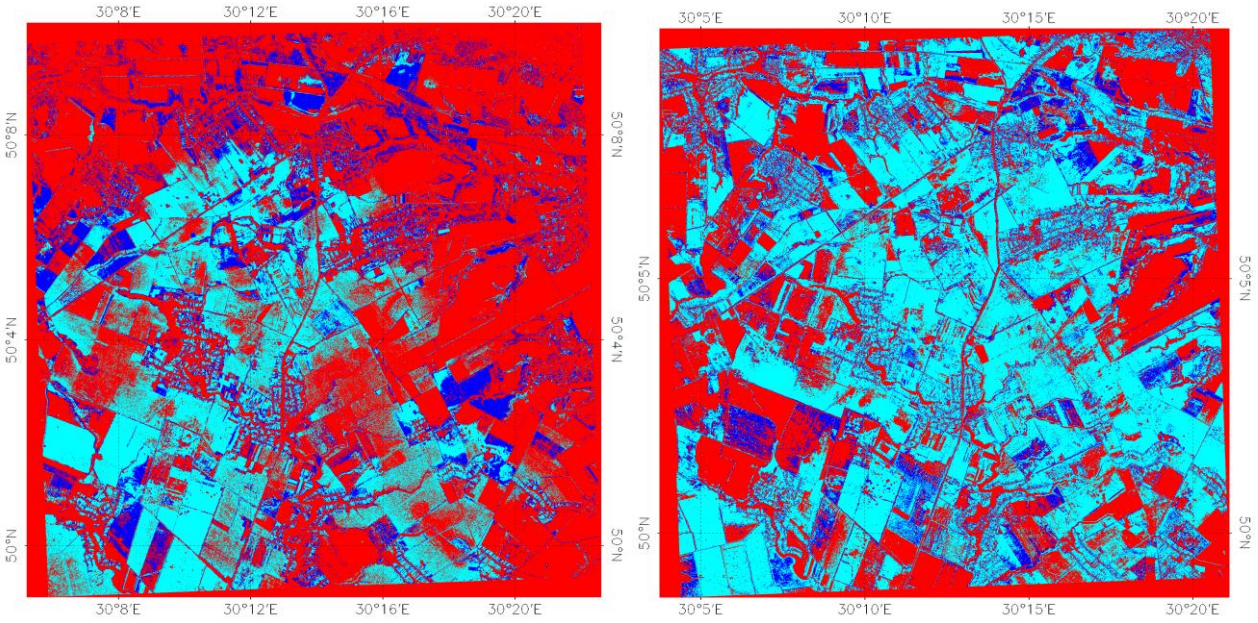

Figure 11: Convex Hull test over 20x20km^2 area centered at the test site: blue clear and dark correspond to the pixels belonging to the ‘strict’ and ‘large’ convex hulls and red to the pixels for which the transfer function is extrapolating. Left: First Campaign (May). Right: Second Campaign (June).

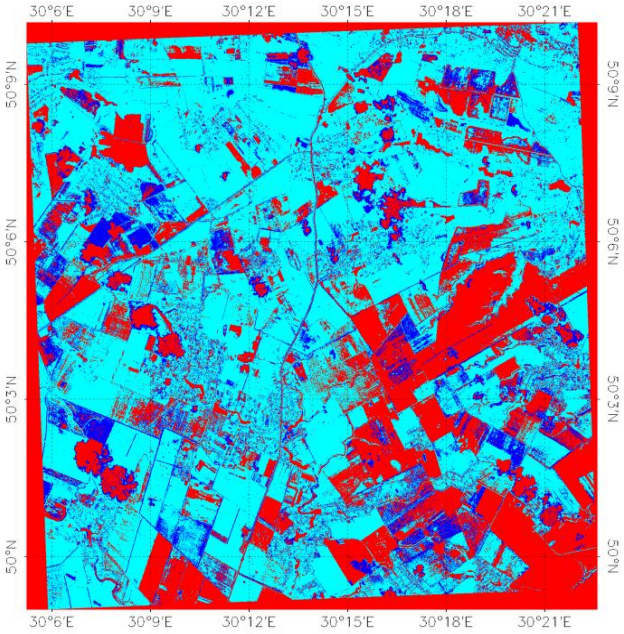

Figure 12: Convex Hull test over 20x20km^2 area centered at the test site: blue clear and dark correspond to the pixels belonging to the 'strict' and 'large' convex hulls and red to the pixels for which the transfer function is extrapolating. Third Campaign (July).

6. ESTIMATION OF THE HIGH RESOLUTION MAPS

6.1. IMAGERY

The SPOT5 images were acquired the 6th May, 9th June, and 9th July 2013 (see Table 4 for acquisition geometry). It corresponds to 4 spectral bands from 500 nm to 1750 nm with a nadir ground sampling distance of 10 m. For the transfer function analysis, the input satellite data used is Top of Atmosphere (TOA) reflectance. The projection is UTM 36 North, WGS-84.

Table 4: Acquisition geometry of SPOT5 HRG 2 data used for retrieving high resolution maps.

SPOT 5 METADATA			
Platform / Instrument	SP05 / HRG 2		
Sensor	OPTICAL 10 m		
Spectral Range	B1(green) : 0.5-0.59 µm B2(red) : 0.61-0.68 µm B3(NIR) : 0.78-0.89 µm B4(SWIR) : 1.58-1.75 µm		
	First Campaign (14th - 17th of May, 2013)	Second Campaign (12th - 15th of June, 2013)	Third Campaign (14th - 17th of July, 2013)
Acquisition date	2013-05-06	2013-06-09	2013-07-09
Incidence angle	0.523316º	-14.959932º	15.847º
Viewing angle	0.304184º	-13.208656º	13.962º
Illumination Azimuth angle	152.426463º	141.643664º	148.382º
Illumination Elevation angle	52.719471º	58.316426º	59.501º

6.2. THE TRANSFER FUNCTION

6.2.1. The regression method

If the number of ESUs is enough, multiple robust regression 'REG' between ESUs reflectance and the considered biophysical variable can be applied (Martínez et al., 2009): we used the 'robustfit' function from the Matlab statistics toolbox. It uses an iteratively re-weighted least squares algorithm, with the weights at each iteration computed by applying the bi-square function to the residuals from the previous iteration. This algorithm provides lower weight to ESUs that do not fit well. The results are less sensitive to outliers in the data as compared with ordinary least squares regression. At the end of the processing, two errors are computed: weighted RMSE (using the weights attributed to each ESU) and cross-validation RMSE (leave-one-out method). As the method has limited extrapolation capacities, a flag image (Figure 8), based on the convex hulls, is included in the final ground based map in order to inform the users on the reliability of the estimates.

6.2.2. Band combination

Figure 13 and 14 show the results obtained for all the possible band combinations using the reflectance. The results are thus selected for LAIeff, LAItrue, FAPAR and FCOVER. Attending specifications of minimal noise and maximal sensitivity it has been chosen band 1(green), band 2 (red), band 3(Near Infrared) and band 4 (Short Wave Infrared). Note that this combination of (1, 2, 3, 4) = (G, R, NIR, SWIR) is selected for all the parameters.

This combination on reflectance was selected since it provides a good compromise between the cross-validation RMSE, the weighted RMSE (lowest value) and the number of rejected points.

6.2.3. The selected Tranfer Function

The applied transfer function for each variable is detailed in Table 5, along with its weighted and cross validated errors.

Table 5: Transfer function applied to the whole site for LAIeff, LAItrue, FAPAR and FAPAR. RW for weighted RMSE, and RC for cross-validation RMSE.

Variable	Band Combination	RW	RC
First Campaign			
LAIeff	2.20+0.024·(SWIR) -0.058·(NIR) -0.007·(R)+0.04·(G)	0.26	0.81
LAItrue	2.84+0.028·(SWIR) -0.075·(NIR) -0.011·(R)+0.057·(G)	0.35	1.19
FAPAR	1.74+0.0081·(SWIR) -0.039·(NIR) +0.005·(R)+0.02·(G)	0.13	0.20
FCOVER	1.49+0.0099·(SWIR)-0.041·(NIR) +0.0084·(R)+0.019·(G)	0.15	0.21
Second Campaign			
LAIeff	-0.2-0.011·(SWIR)+0.0015·(NIR) +0.0084·(R)+0.012·(G)	0.663	0.63
LAItrue	-0.052-0.026·(SWIR)-0.028·(NIR) +0.047·(R)+0.026·(G)	1.070	0.99
FAPAR	-0.17-0.0035·(SWIR)+ 0.0081·(NIR) -0.0015·(R)+0.002·(G)	0.166	0.15
FCOVER	-0.15-0.0028·(SWIR)+0.009·(NIR) -0.0025·(R)+0.00022·(G)	0.149	0.16
Third Campaign			
LAIeff	5.822 - 0.023·(SWIR) - 0.063·(NIR) +0.043·(R)+ 0.017·(G)	0.438	0.409
LAItrue	3.957 - 0.026·(SWIR) - 0.0316·(NIR) +0.031·(R)+ 0.021·(G)	0.532	0.491
FAPAR	1.305 - 0.004·(SWIR) - 0.009·(NIR) +0.007·(R)+ 0.002·(G)	0.083	0.079
FCOVER	1.395 - 0.004·(SWIR) - 0.015·(NIR) +0.011·(R)+ 0.003·(G)	0.162	0.155

May 2013 - First Campaign | **June 2013 - Second Campaign**

Figure 13: Test of multiple regression (Transfer Function) applied on different band combinations. Band combinations are given in abscissa (2=G, 3=RED, 4=NIR and 5=SWIR). The weighted root mean square error (RMSE) is presented in red along with the cross-validation RMSE in green. The numbers indicate the number of data used for the robust regression with a weight lower than 0.7 that could be considered as outliers. Left: First campaign (May). Right: Second campaign (June).

July 2013 - Third Campaign

LAIeff **LAI**

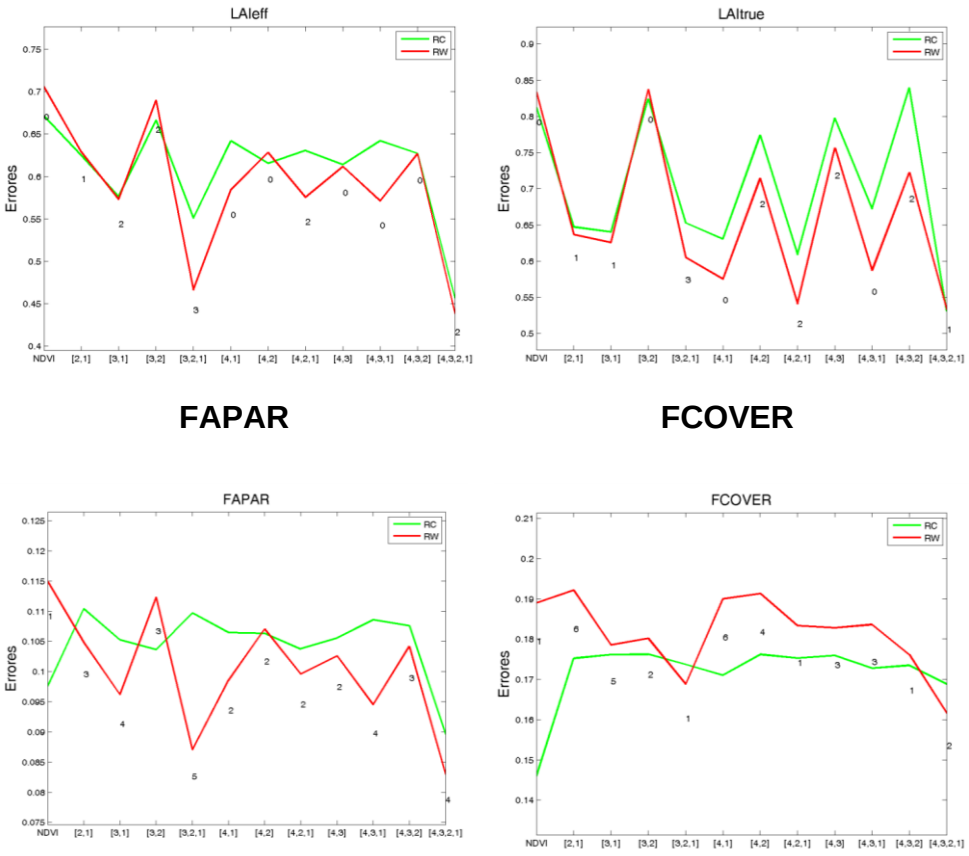

FAPAR **FCOVER**

Figure 14: Test of multiple regression applied (Transfer Function) on different band combinations. Band combinations are given in abscissa (2=G, 3=RED, 4=NIR and 5=SWIR). The weighted root mean square error (RMSE) is presented in red along with the cross-validation RMSE in green. Third Campaign.

May 2013 - First Campaign | **June 2013 - Second Campaign**

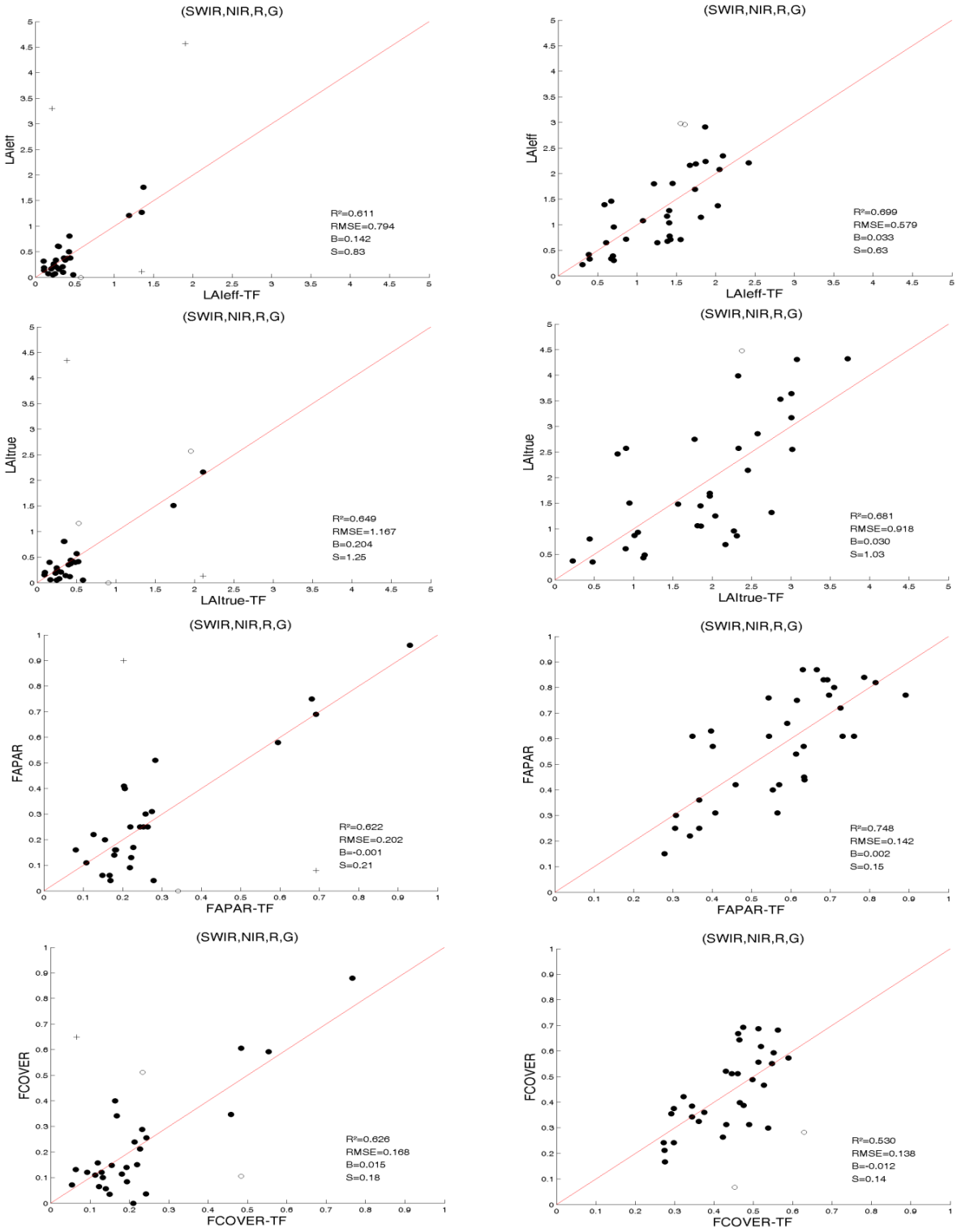

Figure 15: LAIeff, LAItrue, FAPAR and FCOVER: results for regression on reflectance using 4 bands combination. Full dots: Weight>0.7. Empty dots: 0<Weight<0.7. Crosses: Weight=0. Left: First campaign (May). Right: Second campaign (June).

July 2013 - Third Campaign

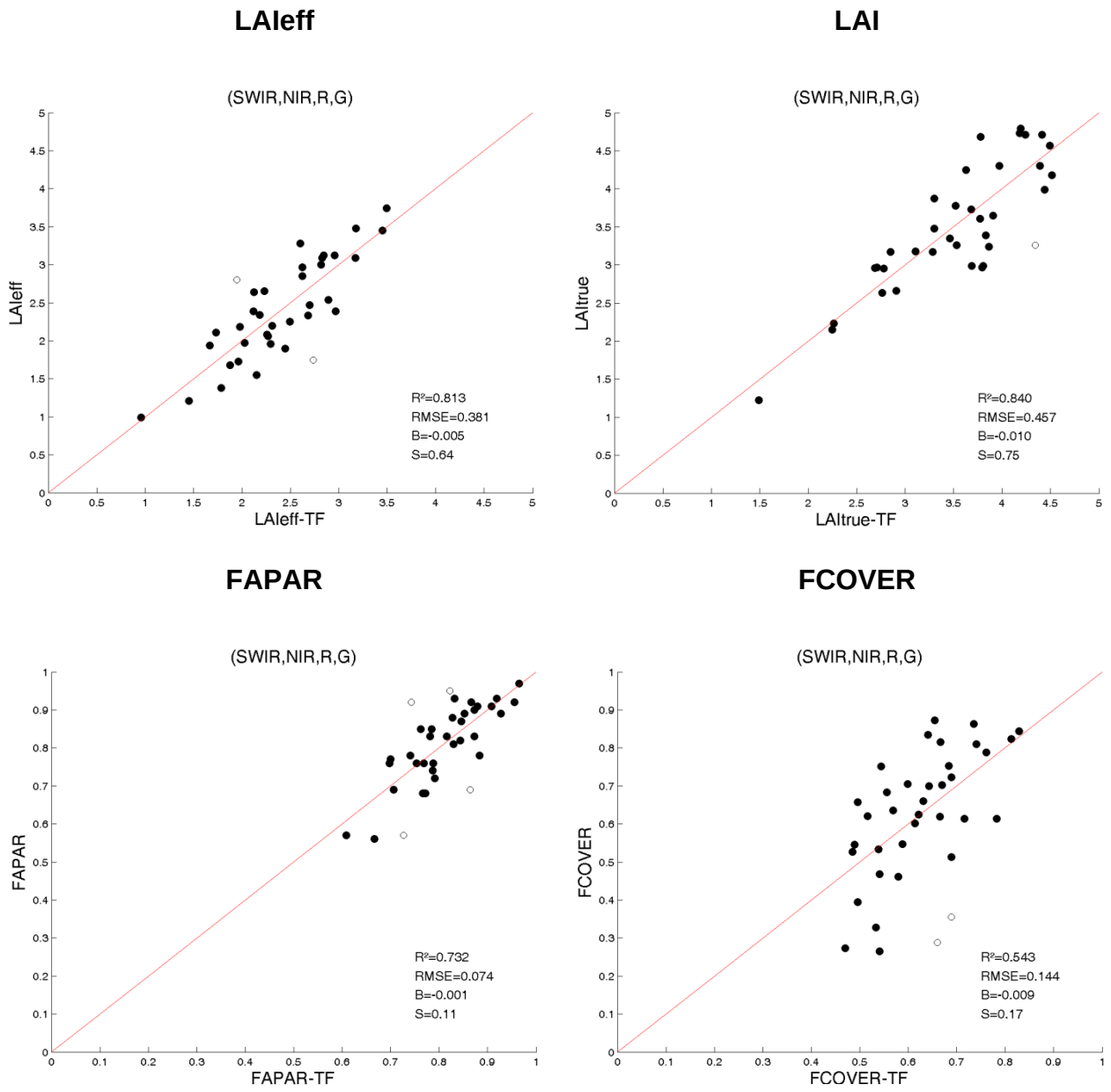

Figure 16: LAIeff, LAItrue, FAPAR and FCOVER. Results for regression on reflectance using 4 bands combination. Full dots: Weight>0.7. Empty dots: 0<Weight<0.7.

Figure 15 and 16 show scatter-plots between ground observations and their corresponding transfer function (TF) estimates for the selected bands combinations. A good correlation is observed for the LAI, LAItrue, FAPAR and FCOVER with points distributed along the 1:1 line. However, for the first campaign the TF estimates present less variability than the ground observations.

6.3. THE HIGH RESOLUTION GROUND BASED MAPS

The high resolution maps are obtained applying the selected transfer function of each variable (Table 5) to the SPOT5 reflectance. Figures 17, 18 and 19 present the TF biophysical variables over 20x20 km^2 extended area. Figure 11 and 12 show the Quality Flag included in the final product.

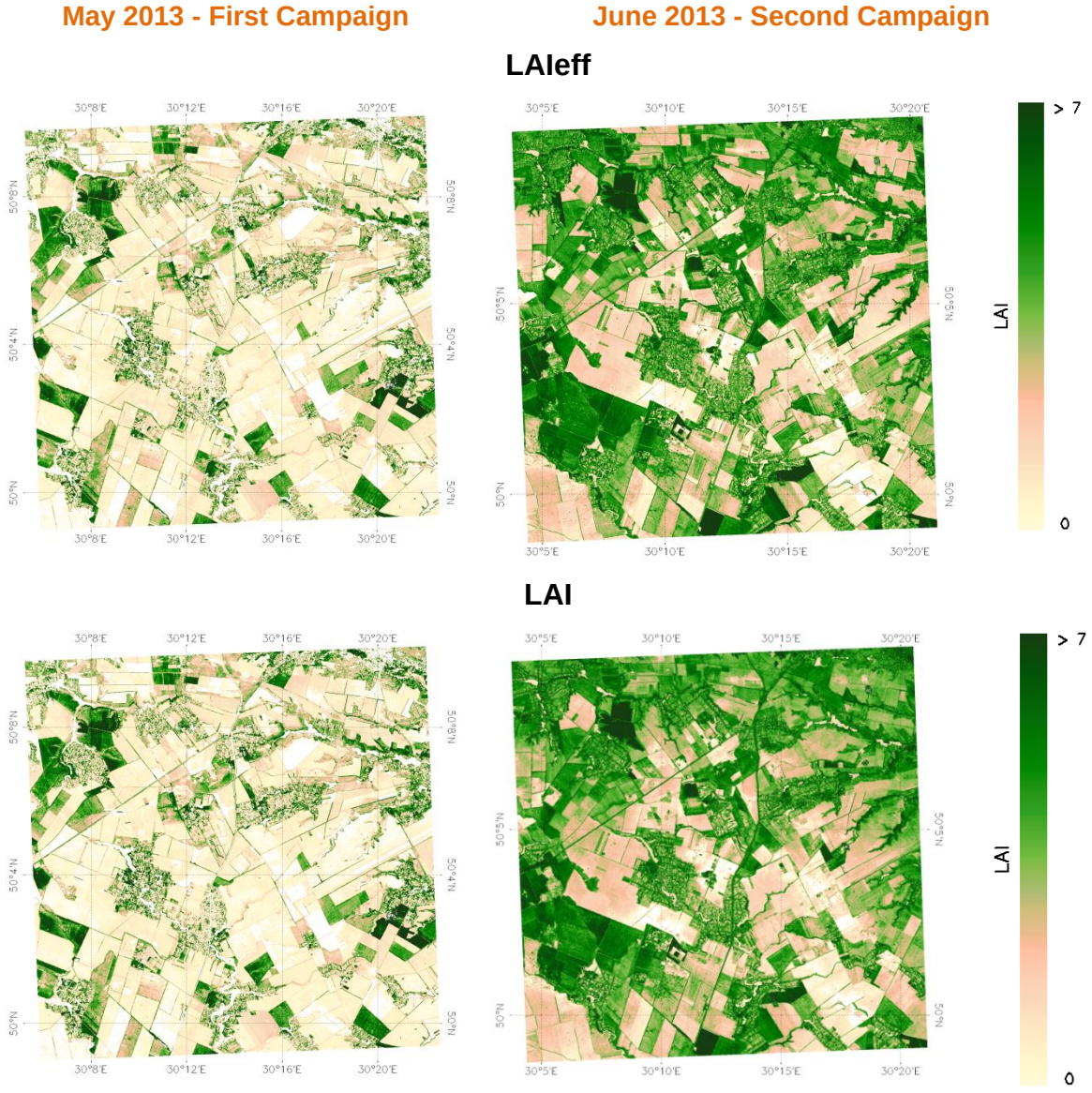

Figure 17: High resolution biophysical maps applied on the Pshenichne site. LAI variables. Left: First campaign (May). Right: Second campaign (June).

May 2013 - First Campaign **June 2013 - Second Campaign**

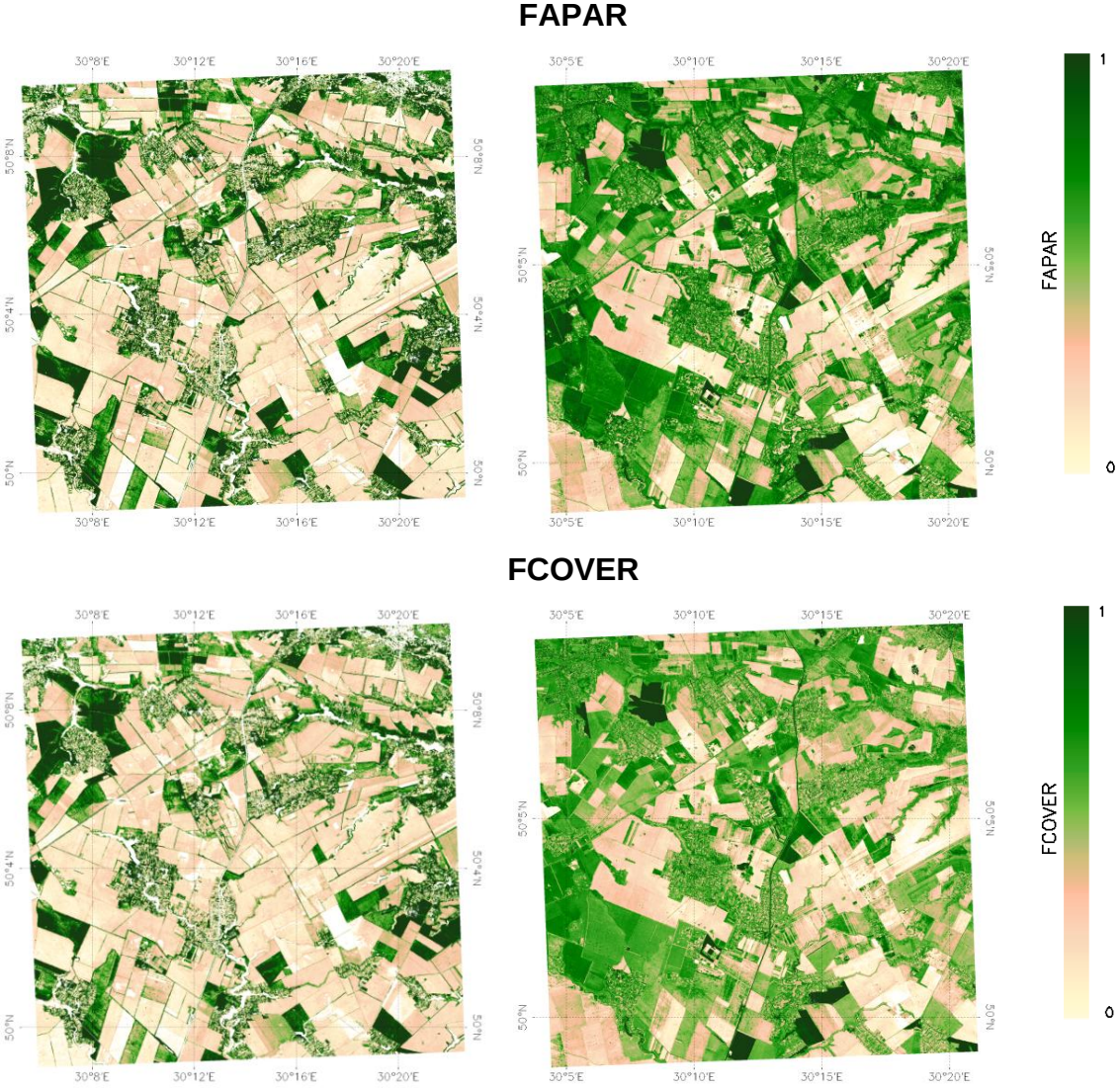

Figure 18: HR biophysical maps applied on the Pshenichne site. Left: First campaign (May). Right: Second campaign (June).

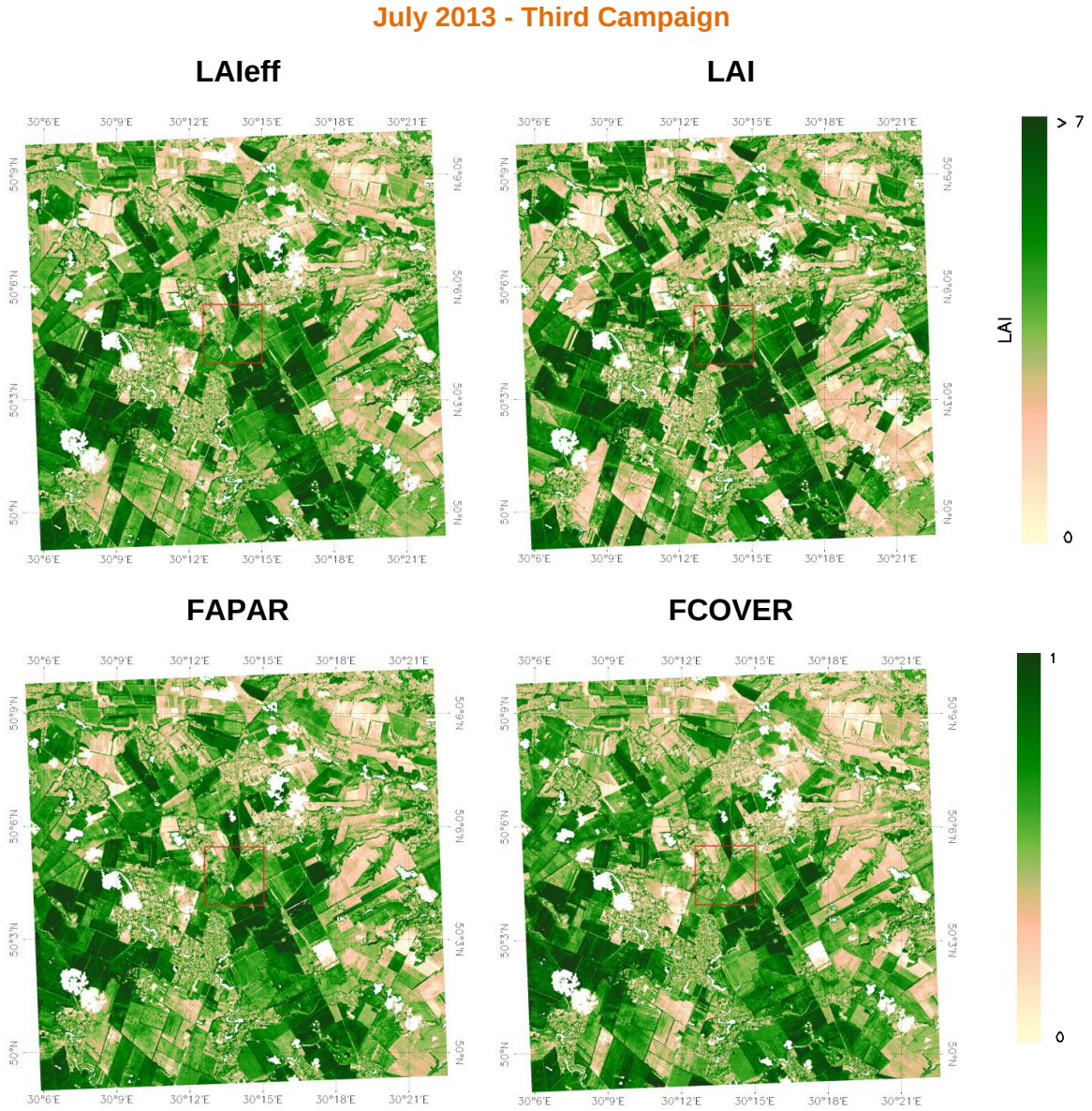

Figure 19: HR biophysical maps applied on the Pshenichne site. Red square corresponds to a 3x3 km area. (White zones: areas where clouds have been removed). Third Campaign (July)

May 2013 - First Campaign **June 2013 -Second Campaign**

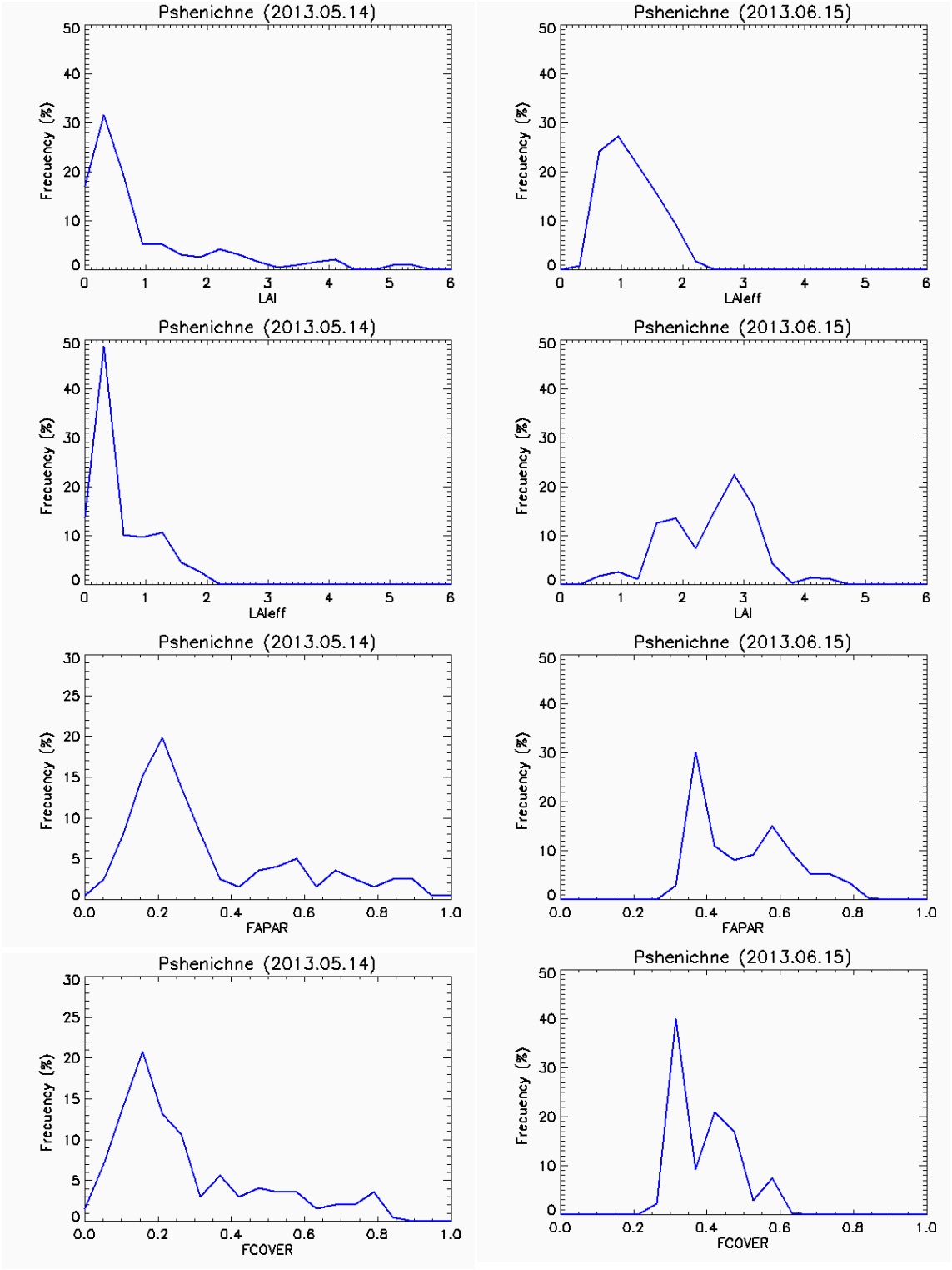

Figure 20: Distribution of the HR biophysical maps applied on the Pshenichne site over the 3x3 km^2 study area. Left: First campaign (May). Right: Second campaign (June).

July 2013 - Third Campaign

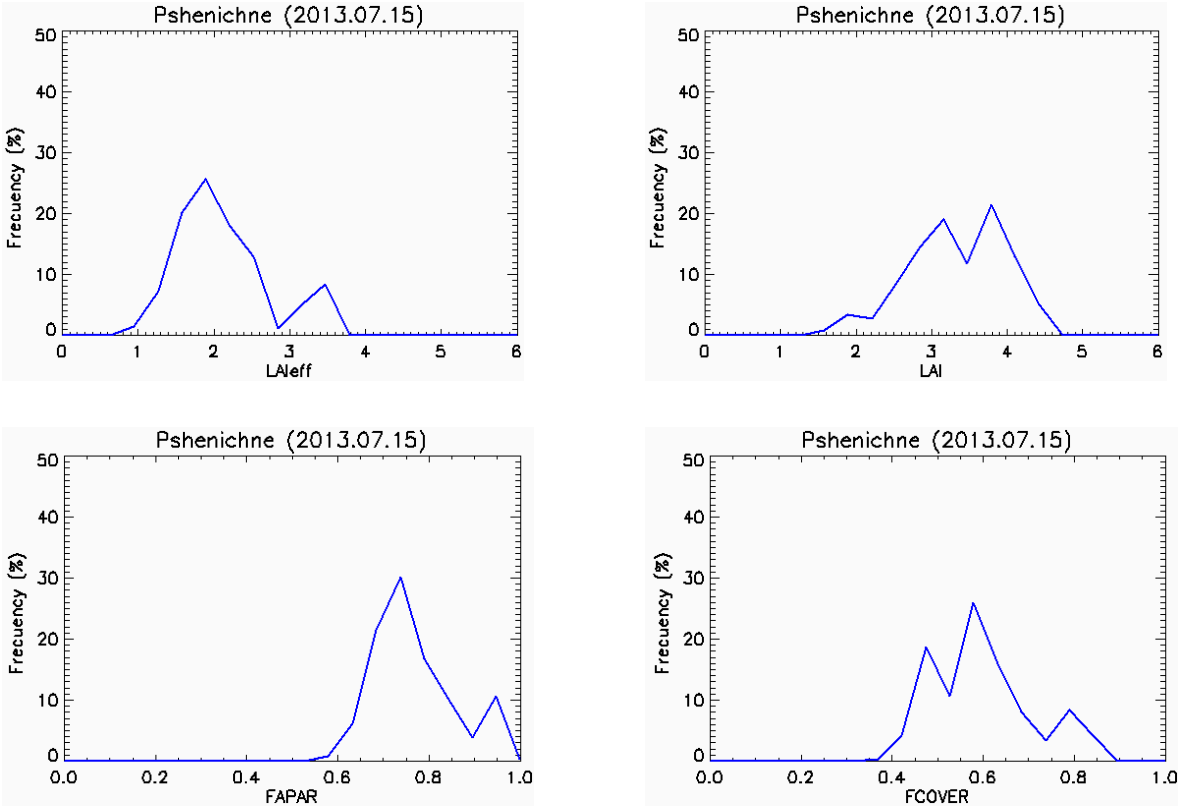

Figure 21: Distribution of the HR biophysical maps applied on the Pshenichne site over the 3x3 km^2 study area. Third Campaign (July).

Table 6 summarizes the mean values for the 3x3 km^2 study area with the same centre. Both maps as the mean values (Table 6), a systematic increase of the vegetation is observed. Figures 20 and 21 show the distribution of values for the 3x3 km^2 study area. The distributions of biophysical maps are consistent with field measurements distributions (figures 7 and 8).

Table 6: Mean values and standard deviation (STD) of the HR biophysical maps for the 3x3km^2 Pshenichne site.

	First Campaign		Second Campaign		Third Campaign	
Variable	Mean	STD	Mean	STD	Mean	STD
LAIeff	0.42	0.39	1.12	0.49	2.42	0.45
LAI	0.57	0.59	1.67	0.81	3.53	0.62
FAPAR	0.26	0.18	0.51	0.13	0.81	0.07
FCOVER	0.21	0.15	0.41	0.08	0.63	0.08

Table 7 describes the content of the geo-biophysical maps in the "SPOT_YYMMDD_Pshenichne_AREA_ETF_BioMap" files.

Table 7: Content of the dataset.

Parameter	Dataset name	Range	Variable Type	Scale Factor	No Value
LAI effective	LAIeff	[0, 7]	Integer	1000	-1
LAI	LAItrue	[0, 7]	Integer	1000	-1
FAPAR	FAPAR	[0, 1]	Integer	10000	-1
Fraction of Vegetation Cover	FCOVER	[0, 1]	Integer	10000	-1
Quality Flag	QFlag	0,1,2 (*)	Integer	N/A	-1

(*) 0 means extrapolated value (low confidence), 1 strict interpolator (best confidence), 2 large interpolator

7. CONCLUSIONS

High resolution maps of main biophysical variables of the vegetation canopy have been derived over the agriculture area of Pshenichne (Ukraine) for three ground campaigns: 14th of May, 15th of June, and 15th of July 2013. Ground data was acquired using digital hemispherical photographs, and processed with CAN-EYE to provide LAI, LAIeff, FAPAR and FCover values. Ground based maps have been derived using high resolution imagery (SPOT-5) according with the CEOS LPV recommendations for validation of low resolution satellite sensors.

The sampling over the study areas was evaluated with the convex hull test. According to this, 73% of the total Pshenichne test site (3x3 km^2) area belongs to the transfer function considered as an interpolator for the first campaign, 83% for the second campaign, and 87% for the third campaign, thus the representativeness of the sampling (i.e., ESUs) over the site is very good.

Transfer functions have been derived by multiple robust regression between ESUs reflectance and the several biophysical variables. The spectral bands combination to minimize errors (weighted RMSE and cross-validation RSME) were band 1 (green), band 2 (red) band 3 (Near Infrared) and band 4 (Short Wave Infrared) combination, for the three campaigns. The RMSE values for the several transfer function estimates are ranging between 0.38 and 0.79 for LAIeff, 0.46 and 1.2 for LAItrue, 0.07 and 0.2 for FAPAR and finally 0.13 and 0.16 for FCOVER. The results are good for the three field campaigns, with no bias and low RMSE.

The biophysical variable maps are available in geographic (latitude-longitude projection WGS-84) coordinates at 10 m resolution. Mean values and standard deviation for LAIeff, LAItrue, FCOVER and FAPAR was computed over the 3x3 km^2 area. LAIeff values ranges between 0.42 in May and 2.42 in July. LAI values range between 0.57 and 3.53, FCover between 0.26 and 0.81, and FAPAR between 0.41 and 0.63, respectively. The distribution of values of the high resolution maps were found consistent with that of the ground sampling. Finally, according to the QF information, the transfer function estimates over the study site are considered reliable.

8. ACKNOWLEDGEMENTS

This work is supported by the FP7 IMAGINES project under Grant Agreement N°311766. SPOT 5-HR imagery are provided through the GMES Services Coordinated Interface (SCI) ESA service. This work is done in collaboration with the consortium implementing the Global Component of the Copernicus Land Service.

Thanks to the Space Research Institute NAS Ukraine and SSA Ukraine for providing the field data.

9. REFERENCES

Baret, F and Fernandes, R. (2012). Validation Concept. VALSE2-PR-014-INRA, 42 pp.

Camacho, F., Cernicharo, J., Lacaze, R., Baret, F., and Weiss, M. (2013). GEOV1: LAI, FAPAR Essential Climate Variables and FCOVER global time series capitalizing over existing products. Part 2: Validation and intercomparison with reference products. *Remote Sensing of Environment, 137: 310-329.*

Demarez, V., Duthoit, S., Baret, F., Weiss, M. and Dedieu, G. (2008). Estimation of leaf area and clumping indexes of crops with hemispherical photographs. Agricultural and Forest Meteorology. I48, 644-655.

Fernandes, R. S. Plummer, F. Baret, G. Schaepman-Strub, J. Nickeson, J. Nightingale (2012). Global LAI Product Validation Protocol, v1.4. Committee of Earth Observing Systems Working Group on Calibration and Validation Land Product Validation Sub-Group (in revision).

Martínez, B., García-Haro, F. J., & Camacho, F. (2009). Derivation of high-resolution leaf area index maps in support of validation activities: Application to the cropland Barrax site. *Agricultural and Forest Meteorology, 149, 130–145*.

Morisette, J. T., Baret, F., Privette, J. L., Myneni, R. B., Nickeson, J. E., Garrigues, S., et al. (2006). Validation of global moderate-resolution LAI products: A framework proposed within the CEOS land product validation subgroup. *IEEE Transactions on Geoscience and Remote Sensing, 44, 1804–1817*.

Weiss, M., Baret, F., Smith, G.J., Jonckheere, I. and Coppin, P., (2004). Review of methods for in situ leaf area index (LAI) determination. Part II. Estimation of LAI, errors and sampling. *Agricultural and Forest Meteorology. 121, 37–53*.